Global Journal of STEM Education & Management Research

Sulfur Dioxide Air Dispersion in the Taal Lake Caldera: An Ordinal Regression Approach and Management Insights from Gaussian Plume Modelling

Jericho A. Trio[1*], Fernando C. Chicano III[2], Patricia Mae M. Clarino[3], Chris C. Guevarra[4]
[1]School of Environmental Science and Management, University of the Philippines Los Baños, Philippines
[2]Division of Physical Sciences and Mathematics, University of the Philippines Visayas, Philippines
[3]Institute of Biological Sciences, University of the Philippines Los Baños, Philippines
[4]Institute of Weed Science, Entomology and Plant Pathology, University of the Philippines Los Baños, Philippines
*Corresponding Author Email: jatrio@up.edu.ph

Received: January 9, 2026
Revised: February 15, 2026
Accepted: March 1, 2026

ABSTRACT

This study investigates sulfur dioxide (SO_2) air dispersion within the Taal Lake Caldera—encompassing Batangas, Cavite, and Laguna—using time-series data from July 2023 to June 2025. By integrating Gaussian plume modeling with logistic regression, the research predicts dispersion odds and simulates volcanic trajectories to inform regional mitigation strategies. Statistical analysis reveals that while rainfall slightly increases the odds of low-range dispersion (OR = 1.0128), increased wind speed significantly expands the dispersion footprint, increasing the likelihood of far-field transport (18–40 km) by 33.77%. Gaussian plume modelling identifies a critical hot zone (0–10 km) where concentrations peak at 3.2 g/m³ due to a topographic pipe effect created by the Tagaytay Ridge and Mt. Malepunyo. This constriction triggers the Venturi effect, preserving high-concentration ribbon plumes that bypass standard lateral dilution. Conversely, mid-field(11–17 km) and dilution (18–40 km) zones exhibit monotonic decay as the plume homogenizes. These findings culminate in a tripartite risk management framework—addressing acute intervention in littoral zones, exposure reduction in mid-field municipalities, and continuous far-field monitoring. The study underscores the necessity of a topographic warning corridor that accounts for terrain-based hazards rather than relying solely on distance-based assessments.

Keywords: airshed, air dispersion, Gaussian plume modelling, ordinal logistic regression, Taal Lake

How to Cite:

Trio, J.A., Chicano, F. C., III, Clarino, P.M., Guevarra, C. C., (2026). Sulfur Dioxide Air Dispersion in the Taal Lake Caldera: An Ordinal Regression Approach and Management Insights from Gaussian Plume Modelling. *Global Journal of STEM Education & Management Research*, 2(1), 22-38. https://doi.org/10.5281/zenodo.18667577

INTRODUCTION

The Taal Caldera Region encompassing the provinces of Laguna, Batangas, and Cavite, is characterized by recurrent activity and potential volcanic hazards. Recent eruptive sequences, specifically the 2020 phreatomagmatic event and the ensuing phases of passive degasification, have yielded substantial observational data concerning the atmospheric transport of volcanic sulfur dioxide. Evaluation of these episodes underscores the nonlinear interactions between emission flux, injection altitude, and regional meteorological parameters in governing the spatial distribution and concentration of air pollutants (Jing et al., 2020). Sulfur dioxide is a primary indicator of magmatic activity, as its release typically corresponds to the ascent of magma toward the surface. During the January 2020 eruption, emission rates surged dramatically, peaking at approximately 5,300 tons per day before tapering to lower levels in the following months (Nee et al., 2024). In contrast to volcanic ash, which has a tendency for speedy settlement due to gravitational pull, gaseous sulfur dioxide can be injected into various levels of the troposphere and even the stratosphere (Koukouli et al., 2022).

In terms of geography, the Taal Caldera is situated on the southwest portion of Luzon, representing a sulfur dioxide point source in the Macolod Corridor (Newhall et al., 1985). The lentic permutations of Taal Lake surround the said volcanic formation. Tectonically, Taal is part of the Luzon Volcanic Arc, driven by the eastward subduction of the South China Sea Plate along the Manila Trench (Delos Reyes et al., 2018). However, its position is further complicated by the interaction of the Philippine Fault Zone and the Lubang Fault, which facilitates the upwelling of magma through localized extensional stresses (Bato et al., 2021). The geology of the Taal region is dominated by a series of caldera-formations that occurred during the late Pleistocene and early Holocene. These events resulted from the catastrophic drainage of shallow magma chambers, leading to the collapse of the overlying volcanic edifice. At least four major eruptions, characterized by extensive ignimbrite deposits and base surges, have been identified as the primary drivers of the current caldera morphology (Moore et al., 1966).

Despite the clear risks, there is a notable lack of site-specific studies regarding the air dispersion of sulfur dioxide air dispersion at Taal. Existing data is derived from satellite-based sensors, such as the TROPOspheric Monitoring Instrument (TROPOMI), which provides a broad-scale overview but often lacks the granularity needed to assess ground-level concentrations within the unique microclimate of the Taal lake-and-caldera system (Jing et al., 2020). Volcanic sulfur dioxide has been detrimental to agriculture as it alters soil chemistry and amplifies the odds for the conception of acid rain (Yang et al., 2009). As a health hazard, inhalation of such an atmospheric chemical triggers irritation in the respiratory tract, often manifesting as coughing, chest tightness, and increased bronchial resistance (Hansell & Oppenheimer, 2004; Whitty et al., 2020). Understanding the behavior of volcanic sulfur dioxide air dispersion will be critical particularly in the development of contextualized policy and site-proximate monitoring measures.

OBJECTIVES OF THE STUDY

The following study seeks to understand sulfur dioxide air dispersion in the Taal Caldera region, specifically this study aims to:

(i) predict the relative odds of sulfur dioxide air dispersion

(ii) simulate the trajectory of volcanic sulfur dioxide and identify potential impact areas

(iii) develop management monitoring plans and associated mitigating measures

The following study is focused primarily on modelling air dispersion of sulfur dioxide in provinces within the circumference of the Taal Caldera Region, namely, in the provinces of Batangas, Cavite, and Laguna. Sulfur dioxide is a critical compound for the formation of particulate matter in episodes of volcanic activity. Constraining the scope of the study on the dispersal behavior of the compound will be crucial in understanding particulate matter mobility. In terms of data limitations, the study is limited to time series data sets provided by PHIVOLCS, EMB-Region IVA, and PAG-ASA. The interval of the time series data is from July 2, 2023 to June 24, 2025.

LITERATURE REVIEW

The Venturii Effect and Bernouilli Principle of Air Dispersion

In modern urban planning, the Venturi Effect is frequently observed as a narrow tube effect taking into conception when prevailing winds enter a narrow street canyon flanked by high-rise buildings, the air is compressed and accelerated (Li et al., 2021). Recent studies using Computational Fluid Dynamics (CFD) have demonstrated that this acceleration is vital for flushing traffic-related emissions, out of pedestrian zones (Yang et al., 2025). Research into high-density urban blocks in urban Asia found that optimizing ventilation corridors based on Venturi principles can reduce local pollutant concentrations by up to 30%

by preventing the formation of stagnant wake vortices (Zhou et al., 2025). Conversely, if building layouts are poorly staggered, they can negate these effects, leading to high-pressure zones that trap contaminants at the street level (Li et al., 2021).

The integration of the Bernoulli's Principle to the Venturi Effect is central to sustainable understanding of sulfur dioxide behavior within urban and peri-urban arrangements. Passive ventilation systems utilize wind-driven pressure differentials to improve indoor air quality (IAQ) without mechanical energy. Wind blowing over a building's roof creates a low-pressure region—an application of Bernoulli's theorem which naturally draws indoor air out through exhaust vents or Venturi cowls (Zhou et al., 2025). During the post-pandemic era, urban ecologists have emphasized these principles to mitigate air pollutant transmission. Recent experiments show that leveraging the pressure gradient between a high-velocity outdoor wind and a relatively stagnant indoor environment can achieve rapid air exchange rates. Specifically, strategically placed openings can utilize the Venturi effect to ensure that "stale" air is expelled through suction rather than just mixing, thereby reducing the residence time of infectious particles (Li et al., 2021).

Meteorology and sulfur dioxide air dispersion

The dispersion of SO_2 from volcanic eruptions is a complex process governed by the interplay between eruptive intensity and local meteorological conditions. Meteorological variables such as precipitation, humidity, temperature, and wind speed are critical variables to be considered on how SO_2 is transported, chemically transformed, and eventually removed from the atmosphere. Wind speed is a crucial component for the dilution of volcanic SO_2. High wind speeds promote rapid advection, spreading the plume over vast distances while simultaneously diluting the concentration of gases near the source. For instance, during the 2024 Icelandic fissure eruption, high-altitude winds transported SO_2 over 1,300 km to Scotland, where ground-level concentrations still reached three times the recommended hourly limit. Conversely, low wind speeds can lead to grounding of the plume, where SO_2 accumulates in topographic lows, posing severe health risks to nearby communities (Whitty et al., 2020; Ukhov et al., 2025).

Precipitation acts as a vital cleansing mechanism through a process known as wet deposition or scavenging. Rain and snow physically intercept SO_2 molecules and sulfate aerosols, removing them from the air and depositing them on the Earth's surface. While this significantly improves air quality (Wang et al., 2023), it leads to the formation of acid rain. In volcanic contexts, the scrubbing of SO_2 by rainfall can drop the pH of local precipitation to as low as 1.9, as observed near Kīlauea, causing widespread damage to vegetation and infrastructure (Whitty et al., 2020). Recent advancements in the WRF-Chem model have improved the parameterization of this wet deposition to more accurately track the mass balance of sulfur in the atmosphere (Ukhov et al., 2025).

Atmospheric humidity plays a vital role in the chemical evolution of the plume. SO_2 is oxidized into sulfate aerosols through two main pathways: gas-phase oxidation (via hydroxyl radicals) and aqueous-phase oxidation. High relative humidity facilitates the latter by providing a liquid medium on the surface of volcanic ash and existing aerosols. In the humid environment of the 2022 Hunga Tonga plume, increased water vapor content was found to accelerate chemical reactions and expand the reactive surface area of aerosols, leading to rapid stratospheric changes (Evan et al., 2023). Under high-humidity conditions, the conversion of SO_2 to sulfate is significantly faster than in dry air, where gas-phase reactions dominate (Martin et al., 2018).

Ambient and plume temperatures dictate the vertical dispersion and lofting of SO_2. The initial buoyancy of a volcanic plume is driven by the temperature difference between the hot gases and the surrounding air. Furthermore, SO_2 is radiatively active; it absorbs ultraviolet and longwave radiation, which causes the plume to heat up and "loft" to higher altitudes (Ukhov et al., 2025). This self-lofting can inject SO_2 into the stratosphere, where it persists much longer than in the troposphere. Recent satellite observations of the 2021 La Soufrière eruption demonstrated how temperature-driven buoyancy and shifting wind directions at the tropopause created complex, multi-layered SO_2 structures (Taylor et al., 2023).

Risk society and volcanic hazards

The concept of a risk society, as pioneered by Ulrich Beck, posits that modern civilization is increasingly defined by its response to manufactured uncertainties—hazards created by the very technological and social progress intended to control them (Gavrilă & Cilento, 2023). When applied to volcanic hazards, this framework suggests that while eruptions are natural phenomena, the resulting "risk" is a social product determined by urban density, institutional communication, and the limits of technoscientific monitoring (Völker et al., 2017).

In the context of reflexive modernity, volcanic hazards are no longer viewed simply as "acts of God" but as manageable variables within a complex social-ecological system. Modern societies rely heavily on sophisticated monitoring networks to mitigate these threats; however, this reliance creates a new form of vulnerability where the failure of technical systems or communication protocols can exacerbate a crisis (Beech, 2021). For instance, the standardization of Volcano Alert Level Systems (VALS) often

struggles to reconcile linear scientific data with the non-linear, pluralistic social contexts of at-risk communities (Fearnley, 2012). This tension illustrates Beck's "organized irresponsibility," where the presence of scientific institutions does not necessarily equate to the effective reduction of societal risk (Rebotier et al., 2019).

Recent research into seismic and volcanic crises, such as the 2025 Santorini-Amorgos events, highlights the critical role of inter-institutional coordination and proactive risk communication in modern governance (Mavroulis et al., 2025). These events demonstrate that risk management is now a "cosmopolitan" endeavor, requiring the integration of national civil protection frameworks with local community engagement (Gavrilă & Cilento, 2023). Furthermore, the "risk society" is characterized by a mismatch between institutional preparedness and individual behavior. While governments invest in mitigation infrastructure, household preparedness remains low due to psychological factors such as risk perception, place attachment, and self-efficacy (Ni et al., 2025). Studies indicate that individuals with strong ties to their residence may prioritize the preservation of their home over evacuation, even when faced with high-magnitude geological threats (Ni et al., 2025).

Volcanic hazards suggest that socioeconomic status still dictates the degree of exposure and recovery capacity (Beck, 2016). In regions like the Philippines and Ethiopia, volcanic activity causes cascading effects—such as land degradation and water contamination—that disproportionately impact livestock and agriculture-dependent populations, thereby deepening existing social inequalities (Teku & Derbib, 2025; Aguilar, 2016). Volcanic hazards in a risk society are not merely geological events but are deeply embedded in political and social structures. Effective disaster risk reduction now requires a transition from a "national gaze" to a "cosmopolitan gaze," integrating diverse forms of knowledge and acknowledging the social dimensions of scientific uncertainty (Gavrilă & Cilento, 2023; Rebotier et al., 2019).

METHODOLOGY

Study site

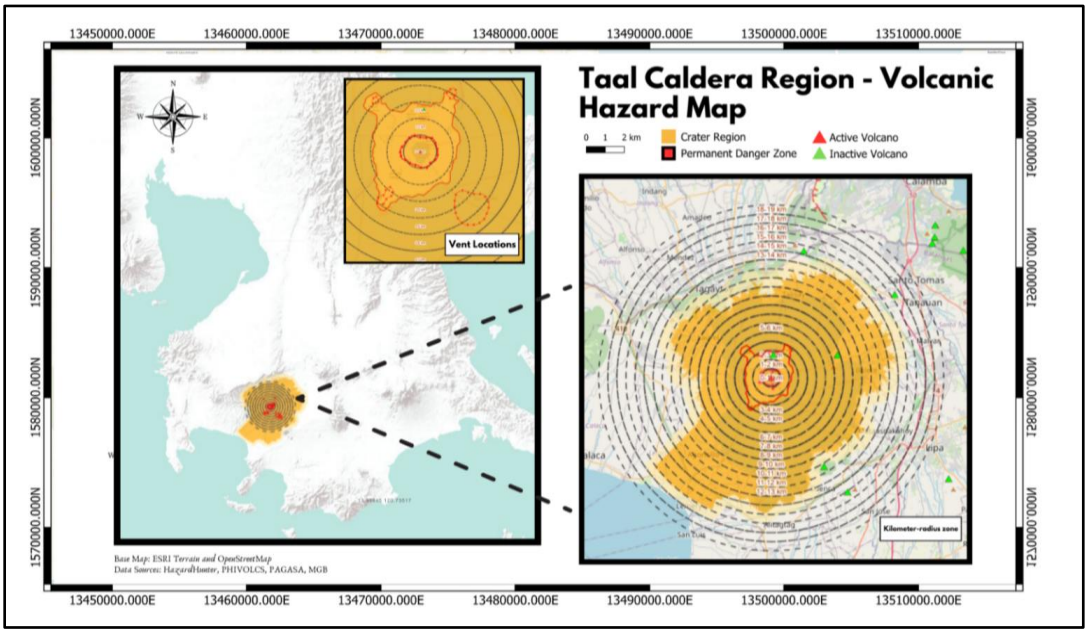

Figure 1. Taal Caldera Region - Volcanic Hazard Map

The Taal Caldera region, located in the intersections of Cavite, Laguna, and Batangas, features a volcanic structure about 25 by 30 kilometers in size. At the center lies Taal Volcano Island, within the expansive 265-square-kilometer Taal Lake. The volcano has been highly active for over 450 years, with major eruptions in 1749, 1754, 1911, 1965, and 2020. These eruptions pose serious dangers including pyroclastic flows and ash fall, particularly affecting lakeside communities west of the island. The caldera's presence in Batangas highlights significant volcanic hazard risks requiring ongoing risk management efforts (Delos Reyes et al., 2018; Lagmay et al., 2021; Balangue-Tarriela et al., 2022).

It is critical to recognize that a caldera region exists as a bowl-like depression that forms when a volcano erupts and subsequently collapses inward. This collapse generally occurs after the magma chamber beneath the volcano empties, removing support for the surface above. Distinguished to a crater, which is typically smaller and formed by explosive volcanic activity ejecting material, a caldera forms due to the structural failure and collapse of the volcano itself. This process results in steep walls and uneven, irregularly shaped edges around the depression (Lipman, 1997; Reynolds et al., 2025).

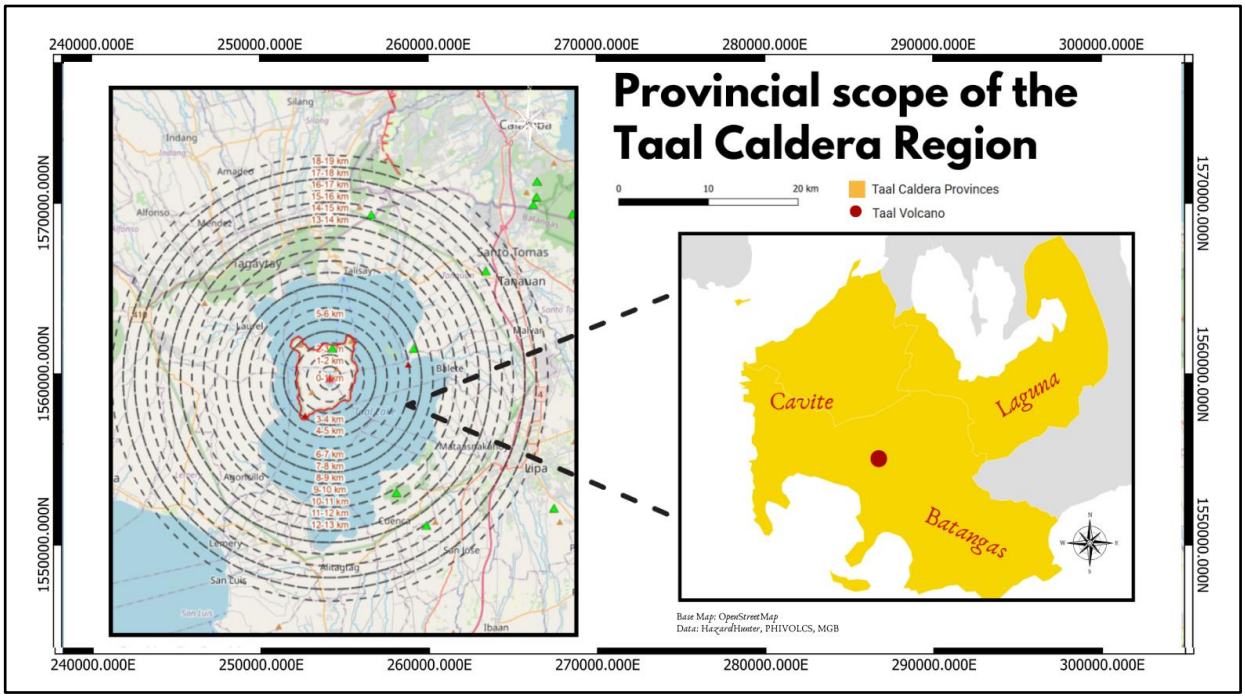

Figure 2. Provincial Scope of the Taal Caldera Region

Gaussian Plume Model

The Gaussian Plume Model (GPM) is a fundamental tool in environmental engineering for assessing point-source dispersion, such as volcanic sulfur dioxide). Rooted in the empirical refinements of Pasquill and Gifford, the model posits that while mean wind advection drives pollutants downwind along the x-axis, turbulent dispersion in the crosswind (y) and vertical (z) planes follows a normal probability distribution (Mao et al., 2020). Due to its computational efficiency, GPM is the standard for regulatory screenings and rapid emergency response, where steady-state assumptions hold true (Holmes & Morawska, 2006).

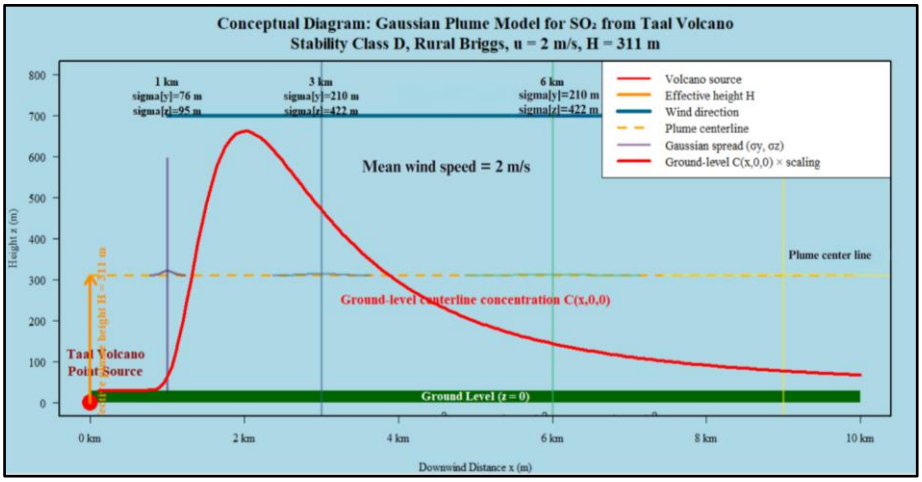

Figure 3. Gaussian Plume Model for Sulfur Dioxide Dispersion from Taal Volcano elevation height of 311 meters (implemented at Stabilly Class D Rural Briggs Classification); illustrated in RStudio 4.5.1)

The simulation in Figure 3, focuses on centerline ground-level concentrations to establish conservative exposure estimates, a critical metric for public health safety. By utilizing Briggs' rural dispersion coefficients—derived for open terrain—and aggregated emission data, the model translates theoretical inventories into actionable dispersion profiles. While the model simplifies complex variable topography, it provides a robust baseline for neutral stability conditions (Class D), effectively balancing mathematical tractability with the accuracy required for preliminary hazard assessment (Hanna & Chang, 1992).

The GPM's mathematical backbone is the three-dimensional concentration field, simplified to ground-level centerline ($\chi(x,0,0)$). The general steady-state advection-diffusion equation under the plume approximation is:

$$\frac{\partial}{\partial x}(u\chi) = \frac{\partial}{\partial y}\left(K_y\frac{\partial \chi}{\partial y}\right) + \frac{\partial}{\partial z}\left(K_z\frac{\partial \chi}{\partial z}\right)$$

Where, χ is concentration (g/m³), u is mean wind speed (m/s), and K_y, K_z exist as eddy diffusivities (m²/s).

Methodological Workflow

The following Gaussian plume model utilized 724 daily measurement sulfur dioxide emissions (in tons/ day) obtained from PHIVOLCS and DENR-EMB Region IV-A. The simulation was implemented with a Wind Speed (u) at 2 m/s and the Effective Stack Height (H)) at 311 meters above sea level (reflecting the height of Taal Volcano). These constants simplify the complex interaction between plume buoyancy and wind momentum. A distance vector (x) is defined ranging from 100 meters to 40 kilometers. This establishes the grid on which the evolution of the volcanic plume will be calculated. An aggregation step was considered (summing the sulfur dioxide measurements) followed by a unit conversion process. This step is critical for dimensional homogeneity, converting the mass flow rate from commercial units (tons/day) into the standard scientific units required by the Gaussian formula (grams/second).

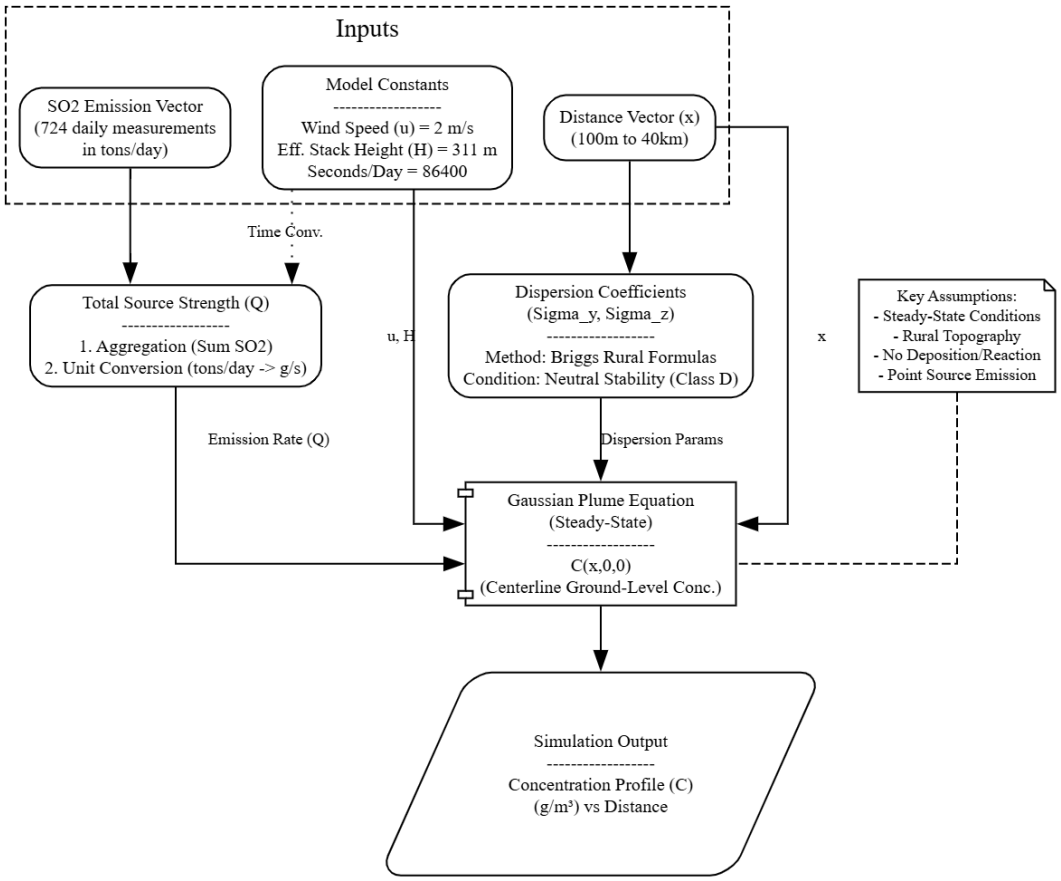

Figure 4. Methodological framework for Gaussian Plume Modelling

A Briggs Rural set-up, appropriate for open terrain, and assumes Neutral Stability (Class D) was implemented. This selection dictates that the plume is modeled under overcast or moderate wind conditions, avoiding the extremes of highly convective (unstable) or stagnant (stable) atmospheres. The framework operates under steady state conditions, assuming that emission rates and wind speeds remain constant over the calculation interval. It assumes rural topography, meaning the dispersion coefficients are not adjusted for urban roughness or heat islands. Furthermore, it assumes non-reactivity, treating sulfur dioxide as a chemically inert tracer that does not fall out of the plume or convert to sulfate particles during the transport time. The final output is the concentration profile. This is a functional relationship mapping pollutant concentration (g/m³) against downwind distance (x). This profile allows to identify the location of maximum impact—the specific distance downwind where the plume hits the ground with the highest intensity—and how quickly the pollutant dilutes as it travels up to 40 kilometers away.

Ordinal logistic regression

The ordinal logistic regression model is given by,

$$logit\big(P(Y \leq j)\big) = log\ log\left(\frac{P(Y \leq j)}{P(Y > j)}\right) = \hat{\alpha}_j - (\beta_1 X_1 + \beta_2 X_2 + \cdots \beta_k X_k)$$

Where k is the number of predictors and $P(Y \leq j)$ is the cumulative probability that the sulfur dioxide stream dispersion falls in category j or below.

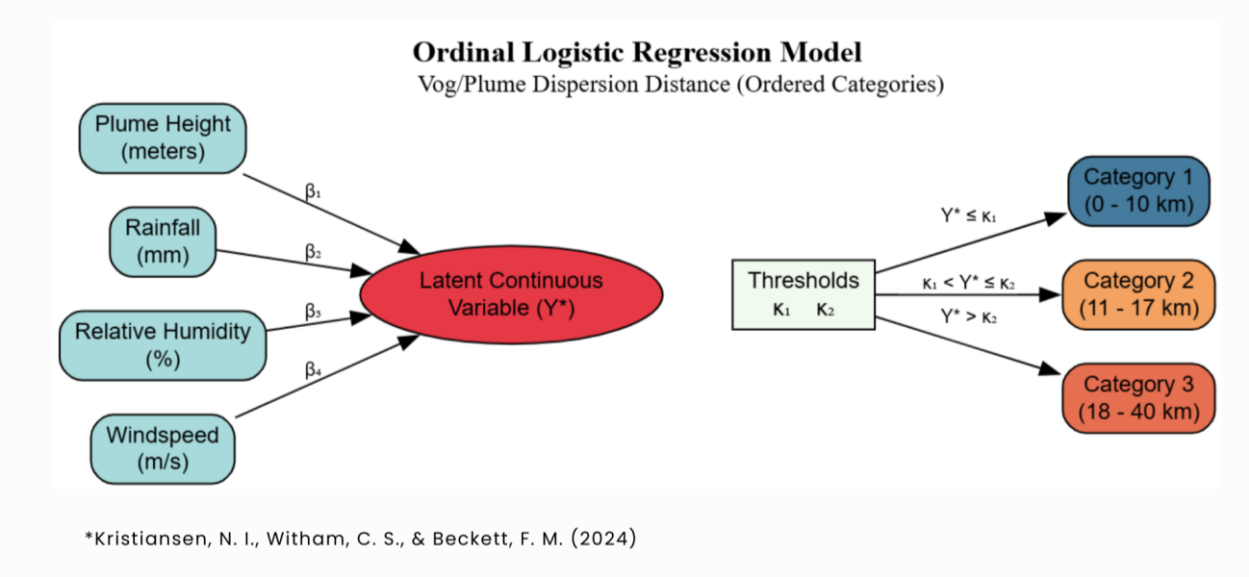

Figure 5. Methodological framework for Gaussian Plume Modelling

Ordinal logistic regression (OLR) is a statistical method for modeling relationships between a nominal dependent variable with multiple ordinal independent variables, which can be either categorical or continuous. OLR is particularly useful when the outcome variable is nominal with inherent order (Fitzhugh et al., 2023). The fundamental equation of the OLR model operates under a natural logarithm of the odds of membership in each category relative to a reference category as a linear function of predictor variables. In the case of this study, the response variable operates under three thresholds on which Gaussian sulfur dioxide plume would behave namely: (i) (0 -10 km - low emission), (ii) (11 - 17 km - medium emission), and (iii) (18 - 40 km - high emission) (Kristiansen et al., 2024). Four predictor variables were assigned in the ordinal logistic regression model, (i) plume height (in meters), (ii) rainfall (in mm/day), relative humidity (in percentage), and windspeed (in m/s).

Diagnostic checks

RStudio 4.5.1 was the software utilized to perform diagnostic checks for model robustness and validity. In terms of the ordinal logistic regression pathway, the following libraries and functions were pursued; for model fitting, the 'MASS' package and the 'ordinal' package (to link cumulative models) were accounted for relationship estimation between predictors and ranked outcomes. The 'sure' package was then incorporated to generate surrogate residuals. Utilizing QQ plots model fitness was verified. For interpretation, the 'ggeffects' package converted log-odds coefficients into marginal effect plots. The 'esquisse' add-in was pursued to rapidly customize visualization via the 'ggplot2' interface. For the Gaussian plume model, the 'openair' package in RStudio was considered to verify the simulations through Taylor diagrams and root mean square error (RMSE).

Ethical considerations

The study did not involve the use of human participants. This study was only limited on secondary data from government institutions such as PHIVOLCS, EMB-Region IVA, and PAG-ASA. Such government bodies were ascertained that the results will only be utilized for academic purposes such as in research, publications, and conference proceedings. Through the conduct of diagnostic checks (see appendix section), the authors of the paper assure that careful handling of secondary data was pursued.

RESULTS AND DISCUSSION

Ordinal logistic regression analysis

The dataset comprises 724 total observations categorized by Sulfur Dioxide Stream Dispersion levels. The distribution is notably skewed toward the middle and higher dispersion distances. Tier 2 (11 - 17 km) represents the largest portion of the sample, accounting for 346 observations (47.79%).

Table 1

Descriptive Statistics of the Categorical Variables

Variable	Frequency	Percent (%)
Sulfur Dioxide Stream Dispersion		
1 (0 – 10km)	94	12.98
2 (11 – 17km)	346	47.79
3 (18 – 40km)	284	39.23

Regarding the continuous meteorological and plume-specific variables, distinct trends were observed across the three sulfur dioxide dispersion tiers. Plume height exhibited a steady downward trend as dispersion distance increased, with the highest mean recorded in Tier 1 (0 – 10km) at 877.66 m (SD = 541.83), decreasing through Tier 2 (M = 802.02 m, SD = 618.00) to a low in Tier 3 (M = 740.67 m, SD = 662.80); notably, plume height maintained a wide range across all tiers, reaching maximums of up to 3,000 m, which indicates significant vertical variability regardless of horizontal dispersion. In contrast, mean rainfall levels showed a positive correlation with dispersion distance, nearly tripling from 2.37 mm (SD = 7.28) in Tier 1 to 6.59 mm (SD = 16.24) in Tier 3 (18 - 40 km), with Tier 2 exhibiting the most extreme precipitation event at 208.40 mm. Relative humidity remained the most stable variable, maintaining high mean levels between 79.48% and 81.74% with minimal variance across all groups, suggesting a consistently moist environment. Finally, mean wind speed demonstrated a steady decline as dispersion distance increased, falling from a peak of 2.65 m/s (SD = 1.18) in Tier 1 to 1.84 m/s (SD = 0.99) in Tier 3, suggesting that shorter dispersion distances are generally associated with slightly higher atmospheric activity.

Table 2

Summary Statistics of the Continuous Variables when grouped according to SO2 Dispersion

Variable	Mean	Std. Dev.	Minimum	Maximum
Plume Height (meters)				
1	877.66	541.832	0.00	3000.00
2	802.02	618.000	0.00	2800.00
3	740.67	662.799	0.00	3000.00
Rainfall (mm)				
1	2.37	7.279	1.00	48.00
2	4.61	16.587	1.00	208.40
3	6.59	16.239	1.00	163.00
Relative Humidity (%)				
1	79.48	6.307	66.00	94.00
2	81.40	6.069	65.00	98.00
3	81.74	5.789	67.00	94.00
Windspeed (m/s)				
1	2.65	1.180	1.00	5.00

2	2.11	1.080	0.00	6.00
3	1.84	0.994	0.00	5.00

Holding wind speed constant, for every millimeter increase in rainfall, the log-odds of falling in or below a given dispersion level decrease by 0.0127, which suggests that higher rainfall slightly increases the likelihood of higher sulfur dioxide dispersion. The odds ratio (OR = 1.0128) further indicates that each millimeter increase in rainfall increases the odds of being in a low dispersion category (0 - 10 km) by 1.28%. Windspeed exhibits a more substantial effect on the outcome. For each 1 m/s increase in windspeed, the log-odds of falling in or below the dispersion level increase by 0.4121, indicating that higher wind speed decreases the likelihood of high sulfur dioxide dispersion levels (18 - 40 km). Conversely, the odds ratio (OR = 0.6623) suggests that for each unit increase in windspeed, the odds of being in a low dispersion category decrease by 33.77%, effectively increasing the likelihood of higher dispersion when rainfall is held constant.

Table 3

Estimation of Model Parameters for the Final Model

Predictors	Estimate	Standard Error	p-value	Odds Ratio
Intercept				
$\hat{\alpha}_1$	-2.7702	0.1943	<0.001	
$\hat{\alpha}_2$	-0.3175	0.1554	<0.041	
Rainfall	0.0127	0.0050	0.011	1.0128
Windspeed	-0.4121	0.0679	<0.001	0.6623

Model Accuracy = 0.490 AIC = 1390.855 BIC = 1409.194 MSE = 0.588 MAD = 0.536

Referencing Table 3, the estimated ordinal logistic regression is derived as follows:

$$logit\left(\hat{P}(Y \leq j)\right) = \hat{\alpha}_j - (\hat{\beta}_1 x_1 + \hat{\beta}_2 x_2)$$

$$logit\left(\hat{P}(Y \leq 1)\right) = -2.7702 - 0.0127x_1 + 0.4121x_2$$

Gaussian plume model

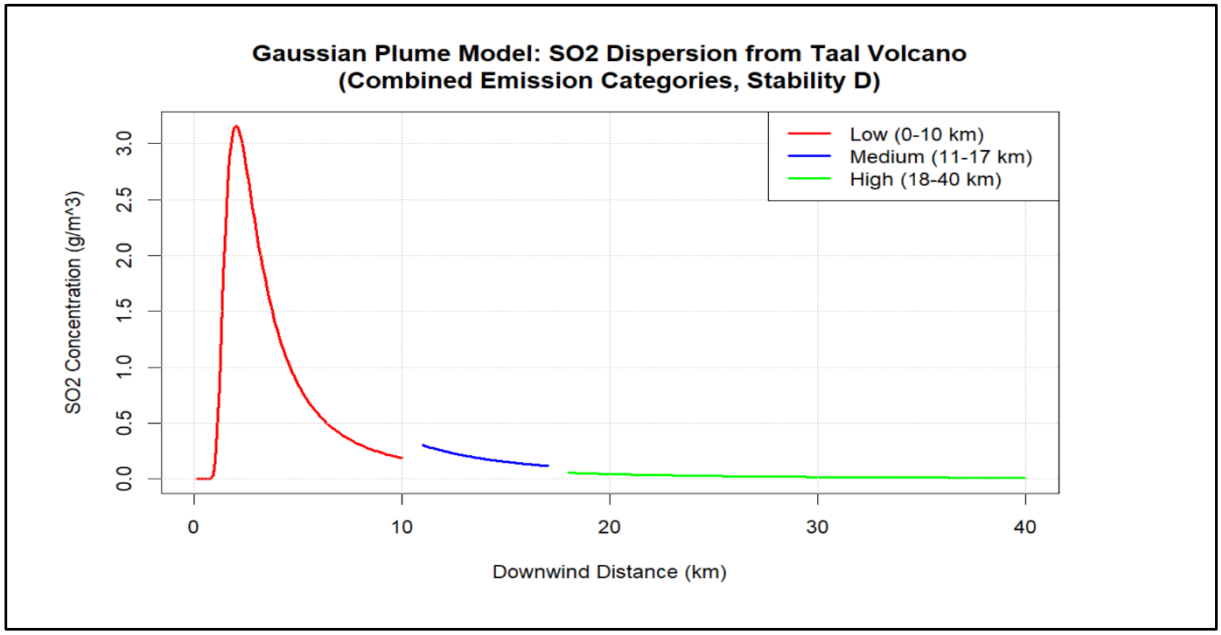

Figure 6. Gaussian Plume Model on Sulfur Dioxide dispersion from Taal Volcano

At near field low sulfur dioxide emissions (0 - 10 km), a classic "hump-shaped" curve is observed —starting near zero, peaking sharply at ~2 km (3.2 g/m³), then decaying rapidly to <0.1 g/m³ by 10 km—capturing Gaussian plume behavior of in a neutral atmospheric stability (Pasquill Class D). It implies a narrow "hot zone" (1–5 km downwind, towards Agoncillo and Laurel lakeshores) with severe exposure. Under these arrangements, neutral stability typically occurs when buoyancy forces are minimized in the environment. Consequently, the pollutant plume does not undergo the erratic vertical oscillations, nor does it maintain a laminar ribbon shape typical of stable inversions (Cooper & Alley, 2011). Instead, the plume expands vertically and laterally at roughly equal rates, forming a cone shape. This expansion follows a Gaussian distribution, driven primarily by mechanical turbulence generated by the wind moving over terrain ruggedness (Zannetti, 1990).

Medium emissions (~601–1,500 tons/day, averaging ~1,387 tons/day) manifest a 11–17 km downwind trajectory from Taal Volcano's main crater. In contrast to the near-field curve segment (0–10 km) with its sharp hump, medium plume emissions manifest a monotonic decay—from ~0.3 g/m³ at 11 km to ~0.12 g/m³ at 17 km. This reflects the plume's "mid-field" phase under neutral stability, where dilution dominates after experiencing peak impingement. Dilution dominates because the cross-sectional area of the plume continues to grow both horizontally and vertically as it travels further downwind. Since the mass flux remains constant, this expansion results in a monotonic decrease in concentration. Within this region, the concentration decay is inversely proportional to the distance (Zannetti, 1990; Vallero, 2025). Key affected areas include Balete, Talisay, and Tanuan.

High emissions (averaging 2,235 tons/day) over 18–40 km downwind, starts 0.056 g/m³ at 18 km and slowly drops to ~0.01 g/m³ by 40 km. At such distances, the volcanic plume is fully mixed with the air. Turbulence has homogenized the plume at such a phase. The concentration does not exist as a function of the release height (311 m); rather, the sulfur dioxide is distributed evenly from the surface to the top of the mixing layer (Turner, 2020). Within these arrangements, risk is flagged as low as it exists below acute health thresholds (<0.001 g/m³ WHO 1-hour limit by ~25 km). Within the 18 - 40 km trajectory, the areas which experience immediate mixing (18 - 25 km), include Santo Tomas (in Batangas), Cabuyao City and Calamba City (in Laguna). The plume concentration drops significantly (approaching 0.01g/m³) and risk is flagged as low 25 - 40 km (flagged as dilution zones). The following areas are identified as dilution areas: (i) Santa Rosa City, (ii) Biñan City, (iii) San Pedro City (in Laguna) and (iv) Muntinlupa City (in Metro Manila).

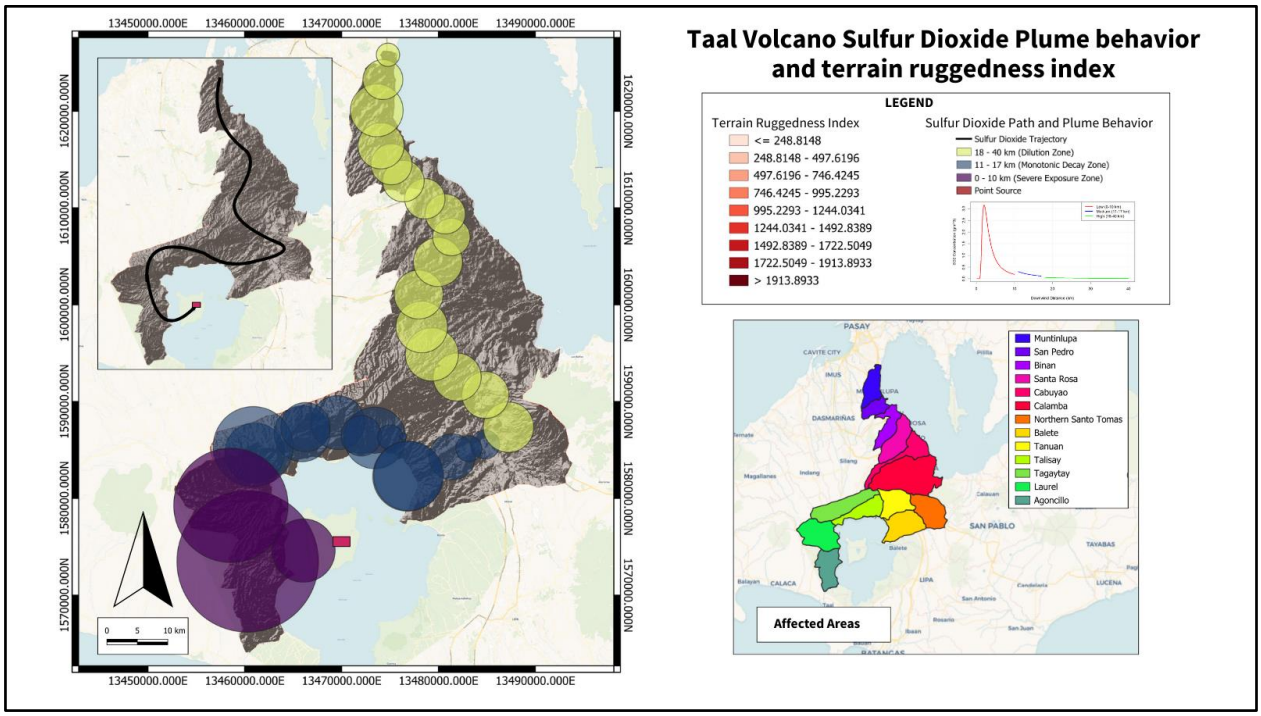

Figure 7. Gaussian Plume Model on Sulfur Dioxide dispersion from Taal Volcano

At the point of emission and immediate transport (0–10 km), the terrain is effectively zero-rugged. The plume is driven purely by the implemented constant wind speed (2 m/s). The direction of the plume may be dictated by the surrounding high ruggedness as the plume cannot easily go westwards (blocked by the 600m high Tagaytay Ridge) or eastwards (blocked by Mt. Malepunyo); rather it is forced northeast. The behavior signifies how high ruggedness steers the intensity into low-ruggedness zones of Laurel and Agoncillo. It is critical to recognize that municipalities are proximate to the Taal littoral lake zone. The reduction of plume mass towards low-rugged zones is anchored within the Venturi effect and the Bernoulli principle; Kossmann and Sturman (2003) explain that winds within a valley are driven by pressure gradients that align with the valley axis. This confines the plume within the valley slopes, preventing lateral dispersion. As a result, the pollutant intensity is preserved. Relative

to the Bernoulli principle, plumes travelling amid the topographic constriction of the Tagaytay Ridge and Mt. Malepunyo do not dilute as expected; instead, they maintain a coherent, high-concentration structure known as a ribbon plume (as evident in the Gaussian plume model in Figure 7 where concentration reaches 3.2 g/m³ at approximately 2 km). The valley floor acts as a pipe, protecting the plume from the turbulent mixing that would otherwise occur if it were exposed to the rougher aerodynamics of the surrounding peaks (Allwine, 1992).

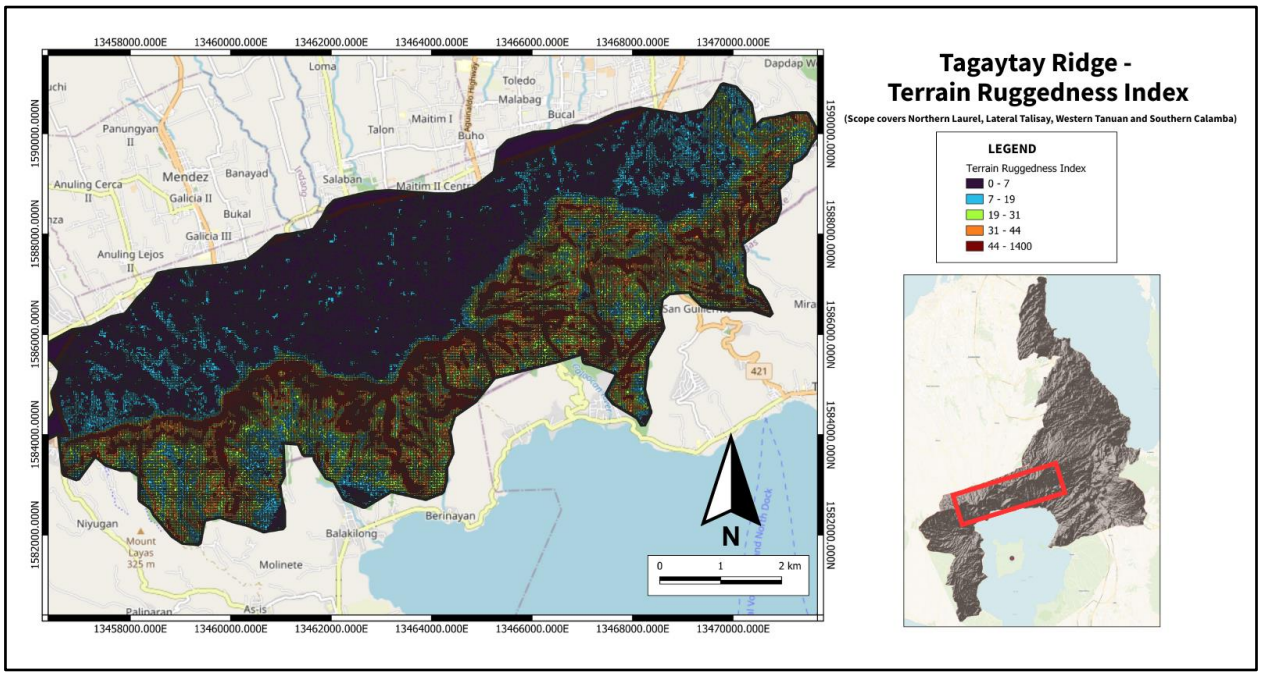

Figure 8. Tagaytay Ridge Terrain Ruggedness Index

Within 11 - 17 km downhill, the following topographic features are evident, namely, the Tagaytay Ridge (whose terrain ruggedness index ranges between 44 - 1400), the footing slopes of Malvar-Balete ridge (whose terrain ruggedness ranges between 20 - 495), and the alluvial fans of Tanuan and Talisay (falling under the terrain ruggedness category of 1 - 15). Referencing Figure 8, it can be observed that the Tagaytay Ridge covers northern Laurel, lateral Talisay, western Tanuan and southern Calamba. Applying the logic of the Venturi effect, the rugged peaks evident in Tagaytay ride may be associated with the trajectory of the plume towards the alluvial zones of Tanuan and Talisay towards the plains of Balete. The northern area of Santo Tomas acts as a vacuum corridor (approximate 18 km downwind from pointsource); relative to its terrain ruggedness index, it can be observed how the area within the foothills of Mount Makiling at the eastern segment of Northern Santo Tomas exhibits elevated undulations (ranging from 39 - 1887). The Santo Tomas corridor is capped in western segment by the Tagaytay ride (TRI of 31 - 1400). Both terrain features constrain the air mass within the valleys and plains of Santo Tomas (TRI of 0 - 5 indicative of flat terrain). This funnels the plume towards the gullies of Calamba.

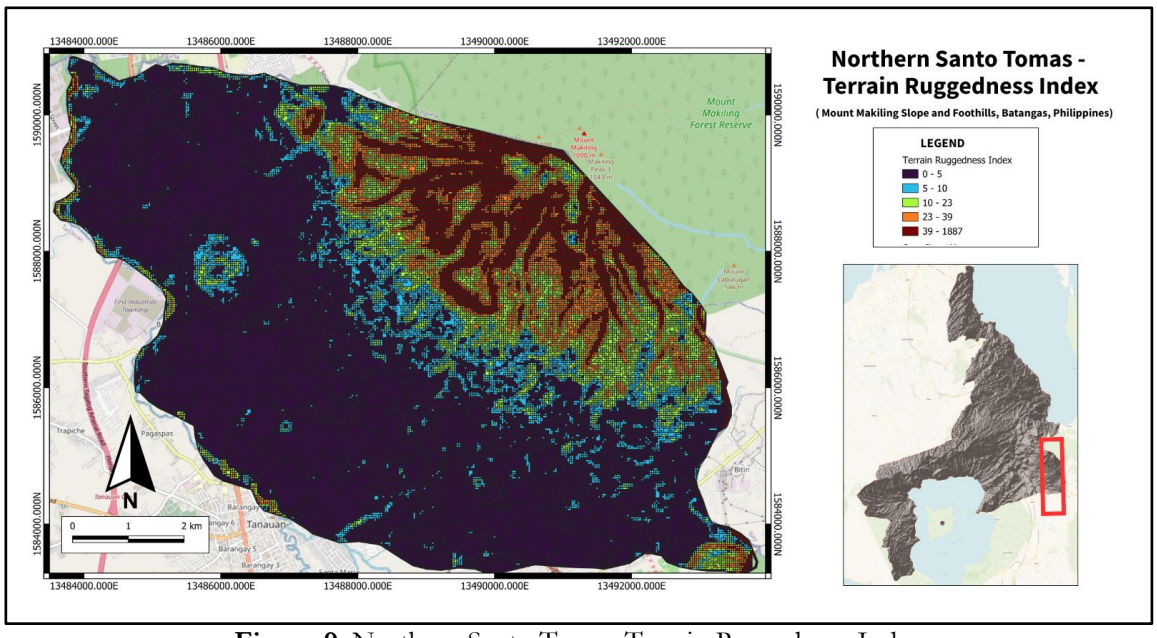

Figure 9. Northern Santo Tomas Terrain Ruggedness Index

The urban arrangements of Calamba, Laguna is characterized by two dominant rugged features, namely, the downstream segment of the San Cristobal River and the entire stretch of San Juan River (whose headwaters originate from the Malepunyo Mountain Range). The persistence of a rugged terrain ranging from 5 - 2179 suggests the persistence of gullies within the river continuum. A rudimentary mechanism by which gullies affect airflow is through the generation and transport of katabatic winds. As defined by Whiteman (2000), gullies within a watershed act as the tributaries of the airshed system. During stable conditions (typically at night or early morning), surface cooling creates a layer of dense, negatively buoyant air adjacent to slopes.

Gravity pulls this dense air down the path of least resistance namely, the gully floor. During periods of neutral stability, gullies function as an aerodynamic roughness factor. Belcher and Hunt (1998) discussed how gullies contribute in drag formation. When prevailing winds blow perpendicular to gullies, flow separation occurs at the windward edge, creating internal recirculating eddies. This phenomenon may trap sulfur dioxide plumes inside the depression, sheltering the compounds from the flushing effect of the main wind field.

Conversely, when winds align with the axis of the gully, the forced channeling effect is wrought into conception. Similar to the larger Venturi effect observed in the Santo Tomas saddle, the gully walls constrain the airflow, reducing lateral turbulence but potentially increasing longitudinal velocity (Kossmann & Sturman, 2003). The area of Calamba is dominated by sulfur dioxide concentrations which are approximately 0.0445 g/m³ suggestive of immediate dilution.

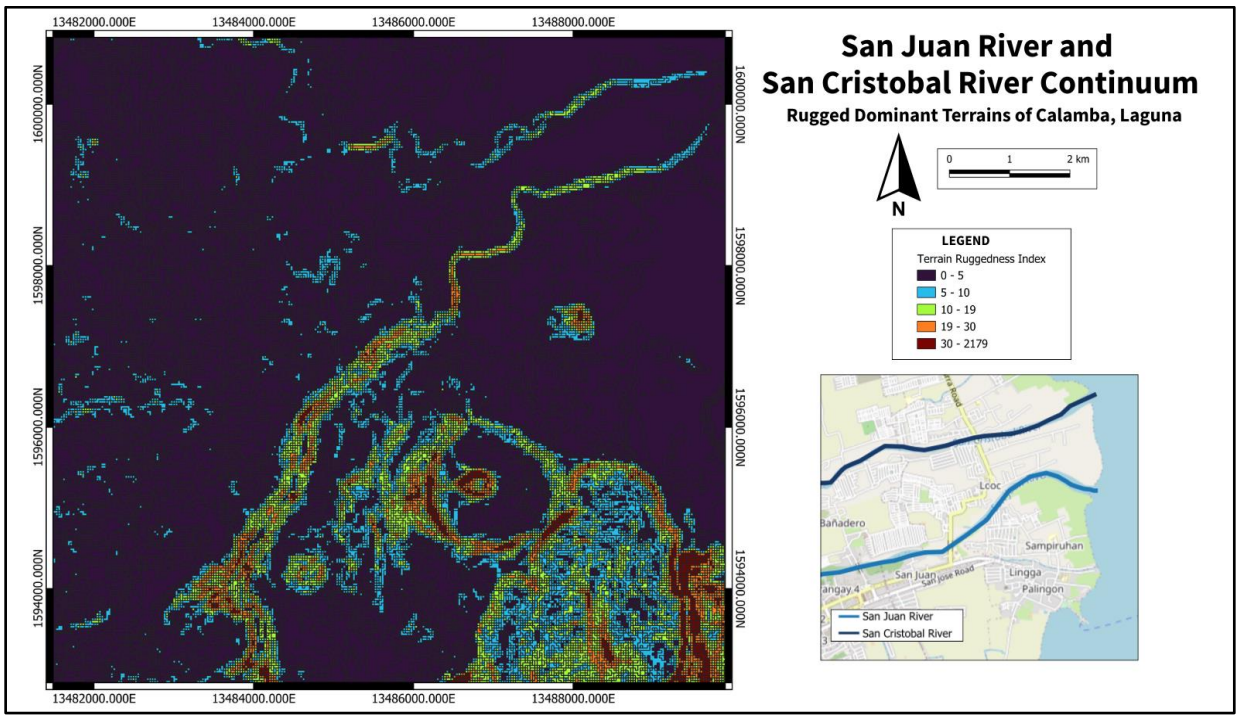

Figure 10. San Juan River and San Cristobal River Continuum Terrain Ruggedness Index

Towards the exit of Cabuyao, the areas of Binan, San Pedro, Santa Rosa, and Muntinlupa are flagged as low risk along the downhill pathway of the Gaussian simulation; these are areas characterized by a terrain ruggedness index value falling within the category of 0 -5 (flat terrain). Air fluid dynamics within Santa Rosa experience an expanded horizontal trajectory (characterized by sulfur dioxide concentration of 0.0188 g/m³).

Plume becomes thinner 35 km downhill (within the areas of San Pedro and Binan), these cities are highlighted by sulfur dioxide concentration of 0.0136 g/m³. As the plume reaches the metropolitan fringes of Muntinlupa, sulfur dioxide homogenizes with the Metro Manila airshed (0.0103 g/m³). To summarize the existing relationships of the Gaussian plume model, a Pearson correlation was utilized between sulfur dioxide concentrations (within the circumference of the projected pathway), distance downhill, and terrain ruggedness index values. The correlation reveals the following:

Table 4

Pearson correlation between downhill distance, sulfur dioxide concentration, and terrain ruggedness (at $p < 0.05$)

Variable	R	p-value	implication
Downhill Distance x SO2 Concentration	-0.549	0.0224	Strong negative
Terrain Ruggedness x SO2 Concentration	-0.421	0.0926	Weak negative
Downhill distance x Terrain Ruggedness	0.491	0.0455	Strong positive

It can be observed how the strong negative association between downhill distance and sulfur dioxide concentration captures the inverse relationship of the Gaussian plume model discussed in Figure 6; the weak negative relationship between terrain ruggedness and sulfur dioxide plume concentration may be expressed by the high heterogenous terrain (standard deviation of 88.065) of the northeast aspect from Agoncillo towards Muntinulpa. Sulfur dioxide plumes tend to cluster in areas with a terrain ruggedness index value of 0 - 5, often characterized by gulleys (San Juan River and San Cristobal River), alluvial fans (Agoncillo, Talisay, Laurel), valleys (Santo Tomas and Balete), and urbanite plains (Cabuyao, Binan, San Pedro, Santa Rosa, and Muntinlupa). The positive relationship between terrain ruggedness and downhill distance from Taal Volcano is exemplified by the flat alluvial fans of Laurel and Agoncillo towards the rugged areas of the Tagaytay ridge, Malvar-Balete ridge, the Mount Makiling slope and foothills, and gulleys of San Juan River and San Cristobal River; thinning as it enters the urbanite flats of Cabuyao onwards.

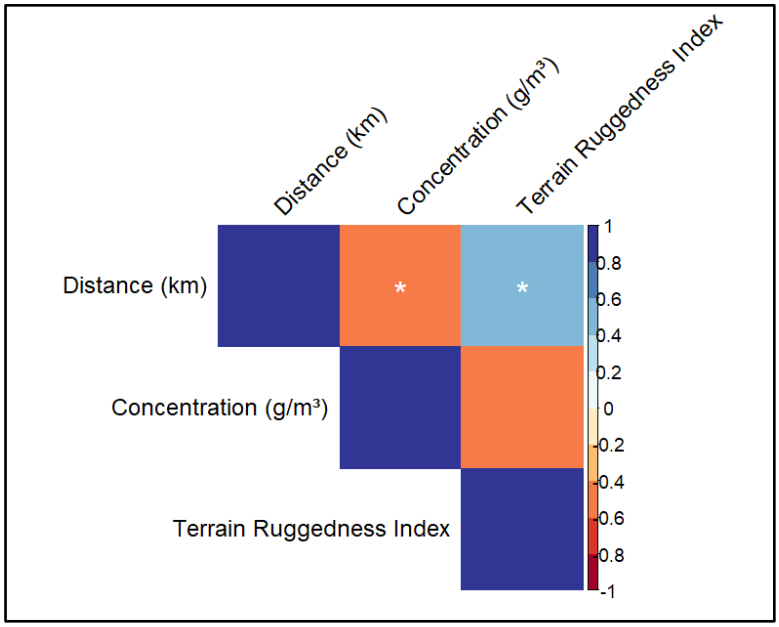

Figure 11. Pearson Correlation Heatmap between terrain ruggedness index (of municipalities and cities covered by the plume trajectory), sulfur dioxide concentration (in g/m³), and downhill distance from the point source (Taal Volcano)

Mitigation and Management Plan

Effective management of volcanic SO_2 emissions in the Taal region requires a tiered monitoring network that prioritizes the ribbon plume behavior identified between the Tagaytay Ridge and Mt. Malepunyo. This surveillance framework operates on four temporal scales: real-time, hourly, daily, and weekly. Real-time automated gas sensors are deployed in the high-risk littoral zones of Agoncillo, Laurel, Talisay, and Balete to track acute SO_2 concentrations. This is supplemented by hourly meteorological assessments at the Taal Volcano Observatory and Tanauan, focusing on wind speed, rainfall, and Pasquill atmospheric stability classes. On a daily basis, these data feed into Gaussian plume models to project trajectories, primarily toward the northeast. Finally, a weekly health surveillance program is established in clinics across Santo Tomas, Calamba, and Cabuyao to monitor longitudinal trends in respiratory distress incidents among the population.

The mitigation strategy is segmented into three distinct risk zones based on dispersion modeling and health thresholds. The hot zone (0–10 km), encompassing the Agoncillo and Laurel lakeshores, requires acute intervention due to severe exposure risks, where concentrations can peak at 3.2 g/m³. In this zone, mandatory evacuation is triggered when emissions exceed 600 tons/ day during low wind speed conditions less than 2 m/s. Infrastructure must be retrofitted as clean air shelters with specialized

SO_2 filtration, and the distribution of full-face respirators is prioritized. The mid-field zones (11–17 km), including Balete, Talisay, and Tanauan, focus on exposure reduction through outdoor activity curfews during Neutral Stability (Class D) events. Additionally, agricultural protection measures are implemented to mitigate soil acidification caused by SO_2 scavenging. Finally, the dilution and mixing zone" (18–40 km), covering parts of Laguna and Metro Manila, maintains vigilance through public health advisories for sensitive groups and continuous sensor monitoring to ensure concentrations remain below the WHO 1-hour limit of 0.001 g/m³.

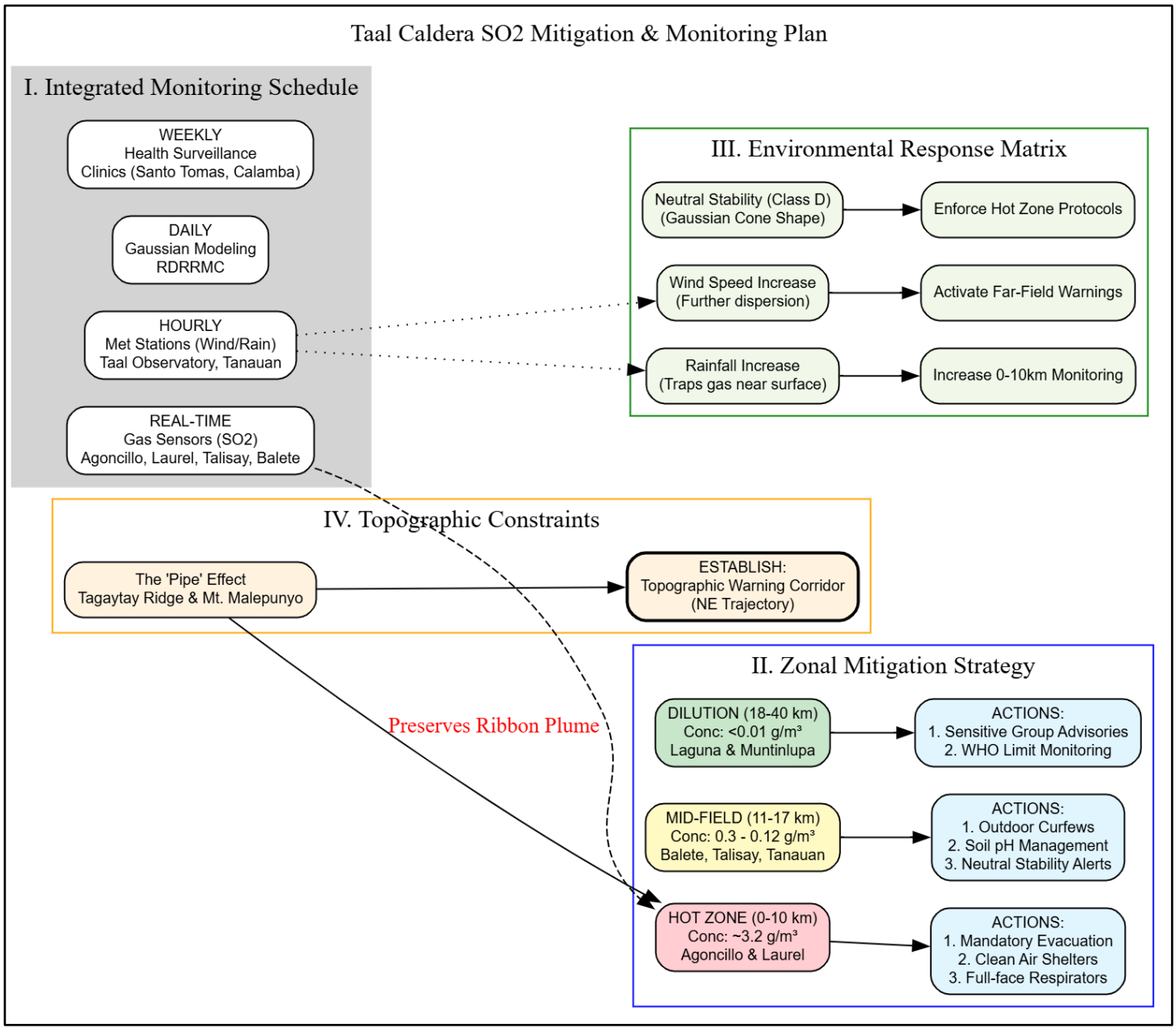

Figure 12. Taal Caldera Region Management Plan centering on Monitoring and Mitigation Measures

The management plan incorporates an adaptive environmental response matrix to account for the impact of rainfall and wind speed on pollutant behavior. Empirical results indicate that rainfall increases the log-odds of SO_2 being trapped in low-range dispersion levels by 1.28%, necessitating intensified monitoring in the 0–10 km littoral zone during wet weather. Conversely, increased wind speed significantly expands the dispersion footprint; each unit increase in wind speed increases the likelihood of the plume reaching the 18–40 km range by approximately 33.77%. This necessitates the activation of early warning systems for far-field urban centers like Calamba and Muntinlupa. Furthermore, during periods of Neutral Stability (Class D), where the plume follows a standard Gaussian cone expansion, hot zone protocols must be strictly enforced regardless of immediate sensor readings due to the predictability of high-intensity impingement.

CONCLUSION

This study demonstrates that SO_2 dispersion within the Taal Caldera region is a complex, nonlinear phenomenon governed by the synergy of emission flux, meteorological forcing, and topographic steering. The findings confirm that the hot zone (0–10 km) remains a region of acute risk, with concentrations peaking at 3.2 g/m^3 under neutral atmospheric stability. A critical discovery is the pipe effect induced by the 600m high Tagaytay Ridge and Mt. Malepunyo, which prevents lateral dilution and funnels high-concentration ribbon plumes toward the northeast. This topographic constriction effectively overrides standard distance-decay models, preserving hazardous air quality far beyond expected limits.

Furthermore, the statistical analysis underscores the role of wind speed as the primary driver for far-field transport, where a 1 m/s increase raises the odds of SO_2 reaching the 18–40 km dilution zone by 33.77%. Consequently, distance-based hazard zones are insufficient without accounting for the Venturi effect and localized terrain ruggedness.

RECOMMENDATIONS

It is recommended that the Philippine government and regional LGUs transition toward a topographic warning corridor framework. This model should trigger high-hazard protocols in the northeast-aligned municipalities whenever volcanic activity escalates, regardless of immediate local sensor readings. Future policy should prioritize the retrofitting of public infrastructure in the hot zone with specialized SO_2 filtration systems and the distribution of full-face respirators. Additionally, an integrated real-time monitoring network—combining PHIVOLCS emission data with PAGASA wind profiles—should be developed to provide automated early warnings for dense urban centers like Calamba and Muntinlupa. Further research is needed to quantify the long-term impact of SO_2 scavenging on the soil chemistry and agricultural yields of the Malvar-Balete ridge to protect the regional economy from volcanic acidity.

Conflict of Interest

The authors of the paper declare no conflict of interest.

REFERENCES

Aguilar, Jr. (2016). Disasters as Contingent Events: Volcanic Eruptions, State Advisories, and Public Participation in the Twentieth-Century Philippines. Philippine Studies: Historical and Ethnographic Viewpoints, 64(3). https://doi.org/10.13185/2244-1638.4182

Allwine, K. (1992). Atmospheric dispersion in mountain valleys and basins. Office of Scientific and Technical Information (OSTI). https://doi.org/10.2172/5814419

Balangue-Tarriela, M. I. R., Lagmay, A. M. F., Sarmiento, D. M., Vasquez, J., Baldago, M. C., Ybañez, R., Ybañez, A. A., Trinidad, J. R., Thivet, S., Gurioli, L., de Vries, B. V. W., Aurelio, M., Rafael, D. J., Bermas, A., & Escudero, J. A. (2022). Analysis of the 2020 Taal Volcano tephra fall deposits from crowdsourced information and field data. Bulletin of Volcanology, 84(3). https://doi.org/10.1007/s00445-022-01534-y

'Bato, M. G., Lundgren, P., Pinel, V., Solidum Jr, R., Daag, A., & Cahulogan, M. (2021). The 2020 eruption and large lateral dike emplacement at Taal volcano, Philippines: Insights from satellite radar data. Geophysical Research Letters, 48(7).

Beck, M. (2016). The Risk Implications of Globalisation: An Exploratory Analysis of 105 Major Industrial Incidents (1971–2010). International Journal of Environmental Research and Public Health, 13(3), 309. https://doi.org/10.3390/ijerph13030309

Beech, D. J. (2017). Managing Volcanic Hazards: An Actor-Network of Technology and Communication (Doctoral dissertation, Aberystwyth University).

Belcher, S. E., & Hunt, J. C. R. (1998). Turbulent flow over hills and waves. Annual Review of Fluid Mechanics, 30(1), 507–538. https://doi.org/10.1146/annurev.fluid.30.1.507

Cooper, C. D., & Alley, F. C. (2010). Air pollution control: A design approach. Waveland press.

Delos Reyes, P. J., Bornas, Ma. A. V., Dominey-Howes, D., Pidlaoan, A. C., Magill, C. R., & Solidum, Jr., R. U. (2018). A synthesis and review of historical eruptions at Taal Volcano, Southern Luzon, Philippines. Earth-Science Reviews, 177, 565–588. https://doi.org/10.1016/j.earscirev.2017.11.014

Evan, S., Brioude, J., Rosenlof, K. H., Gao, R.-S., Portmann, R. W., Zhu, Y., Volkamer, R., Lee, C. F., Metzger, J.-M., Lamy, K., Walter, P., Alvarez, S. L., Flynn, J. H., Asher, E., Todt, M., Davis, S. M., Thornberry, T., Vömel, H., Wienhold, F. G., … Read, W. G. (2023). Rapid ozone depletion after humidification of the stratosphere by the Hunga Tonga Eruption. Science, 382(6668). https://doi.org/10.1126/science.adg2551

Fearnley, C. J., McGuire, W. J., Davies, G., & Twigg, J. (2012). Standardisation of the USGS Volcano Alert Level System (VALS): analysis and ramifications. Bulletin of Volcanology, 74(9), 2023–2036. https://doi.org/10.1007/s00445-012-0645-6

Fitzhugh, N., Rasmussen, L. R., Simoni, A. H., & Valentin, J. B. (2023). Misuse of multinomial logistic regression in stroke related health research: a systematic review of methodology. European Journal of Neuroscience, 58(4), 3116-3131.

Gavrila, M., & Cilento, M. (2022). Memories of the Future. Ulrich Beck, Risk and Prevention: The Difference that Defeats Indifference. Italian Sociological Review, 12(8S), 991-991.

Hanna, S. R., & Chang, J. C. (1992). Boundary-layer parameterizations for applied dispersion modeling over urban areas. Boundary-Layer Meteorology, 58(3), 229–259. https://doi.org/10.1007/bf02033826

Hansell, A., & Oppenheimer, C. (2004). Health Hazards from Volcanic Gases: A Systematic Literature Review. Archives of Environmental Health: An International Journal, 59(12), 628–639. https://doi.org/10.1080/00039890409602947

Holmes, N. S., & Morawska, L. (2006). A review of dispersion modelling and its application to the dispersion of particles: An overview of different dispersion models available. Atmospheric Environment, 40(30), 5902–5928. https://doi.org/10.1016/j.atmosenv.2006.06.003

Jing, F., Chauhan, A., P Singh, R., & Dash, P. (2020). Changes in Atmospheric, Meteorological, and Ocean Parameters Associated with the 12 January 2020 Taal Volcanic Eruption. Remote Sensing, 12(6), 1026. https://doi.org/10.3390/rs12061026

Kossmann, M., & Sturman, A. P. (2003). Pressure-Driven Channeling Effects in Bent Valleys. Journal of Applied Meteorology, 42(1), 151–158.

Koukouli, M.-E., Michailidis, K., Hedelt, P., Taylor, I. A., Inness, A., Clarisse, L., Balis, D., Efremenko, D., Loyola, D., Grainger, R. G., & Retscher, C. (2022). Volcanic SO2 layer height by TROPOMI/S5P: evaluation against IASI/MetOp and CALIOP/CALIPSO observations. Atmospheric Chemistry and Physics, 22(8), 5665–5683. https://doi.org/10.5194/acp-22-5665-2022

Kristiansen, N. I., Witham, C. S., & Beckett, F. M. (2024). A modelling approach for quantifying volcanic sulphur dioxide concentrations at flight altitudes and the potential hazard to aircraft occupants. Journal of Applied Volcanology, 13(1). https://doi.org/10.1186/s13617-024-00144-x

Lagmay, A. M. F., Balangue-Tarriela, M. I. R., Aurelio, M., Ybanez, R., Bonus-Ybanez, A., Sulapas, J., Baldago, C., Sarmiento, D. M., Cabria, H., Rodolfo, R., Rafael, D. J., Trinidad, J. R., Obille, E., & Rosell, N. (2021). Hazardous base surges of Taal's 2020 eruption. Scientific Reports, 11(1). https://doi.org/10.1038/s41598-021-94866-2

Li, Z., Ming, T., Liu, S., Peng, C., de Richter, R., Li, W., Zhang, H., & Wen, C.-Y. (2021). Review on pollutant dispersion in urban areas-part A: Effects of mechanical factors and urban morphology. Building and Environment, 190, 107534. https://doi.org/10.1016/j.buildenv.2020.107534

Lipman, P. W. (1997). Subsidence of ash-flow calderas: relation to caldera size and magma-chamber geometry. Bulletin of Volcanology, 59(3), 198–218. https://doi.org/10.1007/s004450050186

Mao, S., Lang, J., Chen, T., Cheng, S., Cui, J., Shen, Z., & Hu, F. (2020). Comparison of the impacts of empirical power-law dispersion schemes on simulations of pollutant dispersion during different atmospheric conditions. Atmospheric Environment, 224, 117317. https://doi.org/10.1016/j.atmosenv.2020.117317

Martin, E. (2018). Volcanic Plume Impact on the Atmosphere and Climate: O- and S-Isotope Insight into Sulfate Aerosol Formation. Geosciences, 8(6), 198. https://doi.org/10.3390/geosciences8060198

Mavroulis, S., Mavrouli, M., Sarantopoulou, A., Antonarakou, A., & Lekkas, E. (2025). Increased Preparedness During the 2025 Santorini–Amorgos (Greece) Earthquake Swarm and Comparative Insights from Recent Cases for Civil Protection and Disaster Risk Reduction. GeoHazards, 6(2), 32. https://doi.org/10.3390/geohazards6020032

Moore, J. G., Nakamura, K., & Alcaraz, A. (1966). The September 28–30, 1965 eruption of Taal Volcano, Philippines. Bulletin Volcanologique, 29(1), 75–76. https://doi.org/10.1007/bf02597143

Nee, J.-B., Chang, Y.-P., & Wang, C. C. (2024). Remote sensing of eruptions and transport of Taal volcano in January 2020. Applied Optics, 63(18), 4946. https://doi.org/10.1364/ao.524145

Newhall, C. G., Dzurisin, D., & Mullineaux, L. S. (1984, January). Historical unrest at large Quaternary calderas of the world, with special reference to Long Valley, California. In Proceedings of Workshop XIX (pp. 714-742).

Ni, M., Xia, L., Wang, X., Wei, Y., Han, X., Liu, Y., & Pan, S. (2025). Psychological influences and implications for household disaster preparedness: a systematic review. Frontiers in Public Health, 13. https://doi.org/10.3389/fpubh.2025.1457406

Rebotier, J., Pigeon, P., & Metzger, P. (2019). Remettre le contexte social dans l'étude et la gestion des risques. Retours d'expérience d'une recherche interdisciplinaire sur Esmeraldas, Equateur. Cybergeo. https://doi.org/10.4000/cybergeo.31787

Reynolds, S., Rohli, R. V., Johnson, J., Waylen, P., & Francek, M. A. (2025). Exploring physical geography (2nd ed.). McGraw-Hill Education.

Taylor, I. A., Grainger, R. G., Prata, A. T., Proud, S. R., Mather, T. A., & Pyle, D. M. (2023). A satellite chronology of plumes from the April 2021 eruption of La Soufrière, St Vincent. Atmospheric Chemistry and Physics, 23(24), 15209–15234. https://doi.org/10.5194/acp-23-15209-2023

Teku, D., & Derbib, T. (2025). Geological and hydrometeorological hazards affecting livestock production in Ethiopia: a systematic review of impacts, mitigation, and adaptation strategies. Frontiers in Earth Science, 13. https://doi.org/10.3389/feart.2025.1532694

Turner, D. B. (2020). Workbook of atmospheric dispersion estimates: an introduction to dispersion modeling. CRC press.

Ukhov, A., & Hoteit, I. (2025). Enhancing Volcanic Eruption Simulations with the WRF-Chem Model. https://doi.org/10.5194/egusphere-egu25-12830

Vallero, D. A. (2025). Fundamentals of air pollution. Academic press.

Völker, C., Kramm, J., Kerber, H., Schramm, E., Winker, M., & Zimmermann, M. (2017). More Than a Potential Hazard—Approaching Risks from a Social-Ecological Perspective. Sustainability, 9(7), 1039. https://doi.org/10.3390/su9071039

Wang, R., Cui, K., Sheu, H.-L., Wang, L.-C., & Liu, X. (2023). Effects of Precipitation on the Air Quality Index, PM2.5 Levels and on the Dry Deposition of PCDD/Fs in the Ambient Air. Aerosol and Air Quality Research, 23(4), 220417. https://doi.org/10.4209/aaqr.220417

Whiteman, C. D. (2000). Mountain meteorology: Fundamentals and applications. Oxford University Press.

Yang, K., Krotkov, N. A., Krueger, A. J., Carn, S. A., Bhartia, P. K., & Levelt, P. F. (2009). Improving retrieval of volcanic sulfur dioxide from backscattered UV satellite observations. Geophysical Research Letters, 36(3). Portico. https://doi.org/10.1029/2008gl036036

Yang, Z., Du, Q., Yang, Q., Zhao, C., Li, G., Xia, Z., Xu, M., Yuan, R., Li, Y., Xia, K., Gu, J., & Feng, J. (2025). Modeling urban pollutant transport at multiple resolutions: impacts of turbulent mixing. Atmospheric Chemistry and Physics, 25(15), 8831–8857. https://doi.org/10.5194/acp-25-8831-2025

Zannetti, P. (Ed.). (2013). Air pollution modeling: theories, computational methods and available software. Springer Science & Business Media.

Zhou, M., Cao, X., Qiu, W., & Guo, Y. (2025). Enhancing Air Quality in High-Density Cities: Investigating the Link Between Traffic-Related Air Pollution Distribution and Urban Ventilation. Atmosphere, 16(3), 243. https://doi.org/10.3390/atmos16030243

APPENDICES

Assumption Checks

Multicollinearity

Predictor	VIF
Rainfall	1.002408
Windspeed	1.002408

Since the VIF < 5, there is no multicollinearity among the predictors (no correlation between rainfall and windspeed). Therefore, the coefficient estimates are stable and reliable.

	Statistics	df	p
Brant Test (Proportional Odds)	3.33	2	0.190
Likelihood Ratio χ^2	43.43	2	<0.001
Pearson χ^2 (Goodness of Fit)	1417.13	1444	0.688

The ordinal regression model was validated through several diagnostic tests, beginning with the Brant Test, which confirmed that the proportional odds assumption was not violated $(\chi^2 = 3.33, p = 0.190)$, implying that the effects of rainfall and wind speed on Sulfur Dioxide dispersion are consistent across all levels. The model's overall efficacy was established by the Likelihood Ratio Test ($(\chi^2 = 43.43, df = 3, p < 0.001)$, which demonstrated that the inclusion of rainfall and wind speed provided a significantly better fit than an intercept-only model. Furthermore, the Pearson Chi-Square Test $(\chi^2 = 1417.13, df = 1444, p = 0.688)$, indicated a good fit, as the observed frequencies of dispersion categories did not differ significantly from the model's predictions. Despite this statistical significance and adequate fit, the Pseudo-R2 measures were computed to assess the explanatory power of the ordinal regression model. McFadden's R2 = 0.0304, Cox & Snell's R2 =0.0582, and Nagelkerke R2 = 0.0677, suggests that the model explains a small proportion of the variance in Sulfur Dioxide dispersion. Although the variance explained is modest, the likelihood ratio test confirmed that rainfall and windspeed significantly improve model fit.